Experimental Investigation of Detonation Failure and Re-initiation in Non-uniform Compositions

Stéphane BOULAL[1], Pierre VIDAL[1], Ratiba ZITOUN[1], Takuya MATSUMOTO[2], Akiko MATSUO[2]

[1] Institute Pprime (UPR 3346 CNRS), Fluid Thermal and Combustion Sciences Department
ENSMA, 86961 Futuroscope-Chasseneuil, France
[2] Keio University, Department of Mechanical Engineering
Yokohama, Kanagawa 223-8522, Japan

1 Introduction

In many situations of practical interest, accidental or intentional reactive mixtures show non-uniformities of composition. For example, the explosive clouds formed with the air after leaks of hydrogen in nuclear power plants or of fuel from tanks or ducts involve spatial distributions of composition. In detonation engines such as Pulsed Detonation Engines (PDE) or Rotating Detonation Engines (RDE), the mixture non-uniformities are due to (i) the imperfect mixing resulting from the separate injection of the fuel and of the oxidizer, and to (ii) the presence of residual burnt gases. These are considered as important issues in the development of detonation engines and as one of the causes of the difference between predicted and measured performances [1, 2]. Non-uniform mixtures in a PDE have been quantitatively investigated in [3]. Rankin et al. [4] performed visualizations of the flow field inside a non-premixed RDE, but they could not discuss the influence of the composition non-uniformities. Burr and Yu [5] have considered an unwrapped RDE with an axial injection comprised of a tube equipped with discrete cross-flow injectors of hydrogen and oxygen and initially filled with argon. They observed unsteady dynamics such as detonation failure and re-initiation. Only recently, non-uniformities have been considered in numerical models of RDE, e.g., [6–8]. All works agree with the importance of achieving the best mixing of the reactants to get as close as possible to the ideal detonation properties.

From the fundamental viewpoint, it should be acknowledged that all applications involve complex and specific interplays between 3D composition and temperature gradients. Therefore, progress in understanding and modelling detonation dynamics for these non-ideal conditions should first address more generic 1D configurations of gradients. Several authors have studied detonation dynamics in non-uniform compositions with composition gradients normal or parallel to the direction of detonation propagation, e.g., [9, 10], respectively. Recently, we have considered pa-rallel composition gradients with monotonic distributions of the Equivalence Ratio (ER) going from rich, stoichiometric or lean compositions to leaner ones [11–13]. Detonation dynamics was found to depend on the steepness of the composition distribution and on the local and initial values of the ER, and two me-chanisms for detonation failure were identified. Sudden failure (i.e., shock-flame decoupling) of an initially multicellular self-sustained (Chapman-Jouguet, CJ) detonation was observed with large gradients, and progressive failure through marginal propagation modes, with decreasing number of transverse waves, was obtained with small gradients. We proposed a predictive criterion according to which the non-dimensional number $D\nabla t_c$ should be larger than 1 in order that sudden detonation failure occurs (D the detonation wave velocity, t_c the characteristic time of the Zel'dovich–von Neumann–Döring (ZND) reaction zone, and ∇t_c the spatial derivative of t_c in the direction of the detonation propagation). Thus, values of $D\nabla t_c$ smaller than 1 are necessary conditions for the stable propagation of a multicellular detonation wave. If, subjected to a composition gradient that induces a reactivity decrease, $D\nabla t_c$ becomes larger than 1, then failure through shock-flame decoupling is obtained. Here, we summarize a non-trivial extension of these experimental results for parallel composition gradients to the case of non-monotonic distributions of ER. We interpret our observations according to the generic classification of detonation unsteady phenomena, i.e., supercritical, subcritical and critical behaviors, as observed in experiments of detonation transmissions from a tube to a large volume [14], detonation interactions with boundaries or obstacles [15] or direct initiations of detonations by a sudden energy release [16]. Finally, we show that the proposed criterion for predicting sudden failure through shock-flame decoupling again applies.

2 Experimental set-up

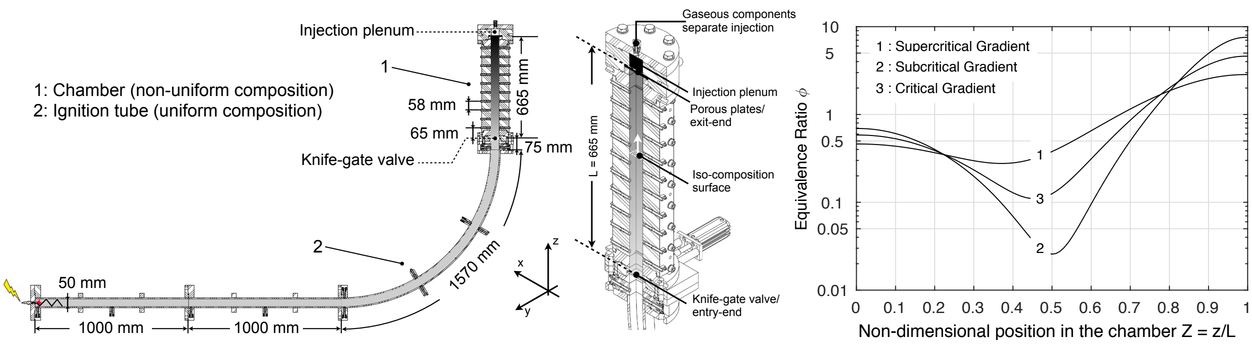

Figure 1: Left: experimental set-up. Center: details of the chamber. Right: non-monotonic ER distributions of $C_3H_8/O_2/C_2H_6$ ($P_0 = 200$ mbar, $T_0 = 290$ K, $L = 665$ mm).

Figure 1 (left) shows schematics of our experimental set-up [11, 12]. The first part (1) is a $50{\times}50$-mm^2-square cross-section, 665-mm-long vertical chamber in which composition gradients are generated, controlled and quantitatively determined (Fig. 1, center). The second part (2) is a 3570-mm-long ignition tube with the same square section as the chamber, and filled with the $C_3H_8 + 5O_2$ uniform detonable composition. The chamber (1) and the ignition tube (2) are separated by a knife-gate valve that was closed during the generation of the non-uniform distribution in (1) and opened just before detonating the uniform mixture in (2). This detonation was classically generated by Deflagration-to-Detonation Transition, with flame ignition from an automative spark plug and flame acceleration enhanced by a 50-cm-length Shchelkin spiral.

The non-uniform, non-monotonic distributions in the chamber were obtained by means of three successive, automated, injections, one for each of the three gases $C_3H_8 + 5O_2$, O_2 and C_2H_6 and then by letting molecular diffusion act. These gases were injected into the chamber (1) from a plenum located at the exit-end of (1) in the decreasing order of their densities in order to suppress Rayleigh-Taylor instabilities. A stack of two porous plates was used to separate the plenum and the chamber (1) in order to suppress the turbulent effects that would have resulted from a point-injection, thereby ensuring surface filling of the chamber. The gradients were controlled by the diffusion time and the ER distributions were determined with oxygen probes coupled with an injection-diffusion 1D numerical model [11, 12]. We have considered three distributions with decreasing then increasing ER, that distinguished from one another by the depth of the reactivity sink, i.e., the difference between the initial and the lowest ER values. Figure 1 (right) shows the non-uniform, non-monotonic distributions thus considered in this study. The initial pressure and temperature in the chamber (1) and in the ignition tube (2) were identical to within 2%, i.e., $P_0 = 200$ mbar and T_0 = 290 K regardless of the distribution in the chamber. The velocity measurements showed that the composition step across the knife-gate valve led to a transient overdriven detonation in the chamber which however relaxed rapidly to the local CJ regime, i.e., $\lesssim$ 10 cm from the chamber entry-end.

We have implemented three measurement techniques to characterize the detonation dynamics in the chamber. The first was a set of ten Kistler 603B piezoelectric pressure transducers, each one paired with a Kistler 5018A electrostatic charge amplifier. They were used to measure the wave longitudinal mean velocity D (not presented here, cf. [12]). The second was the classical sooted-plate technique implemented in the form of a 1-mm-thick stainless steel foil positioned along one inner face of the chamber. The third was Schlieren visualizations across the 50-mm-transverse path of the chamber recorded with a HPV-2 and a HPV-X2 ultra-high speed cameras used with 1-MHz and 5-MHz recording frequencies and 250-ns and 110-ns exposure times, respectively.

3 Results

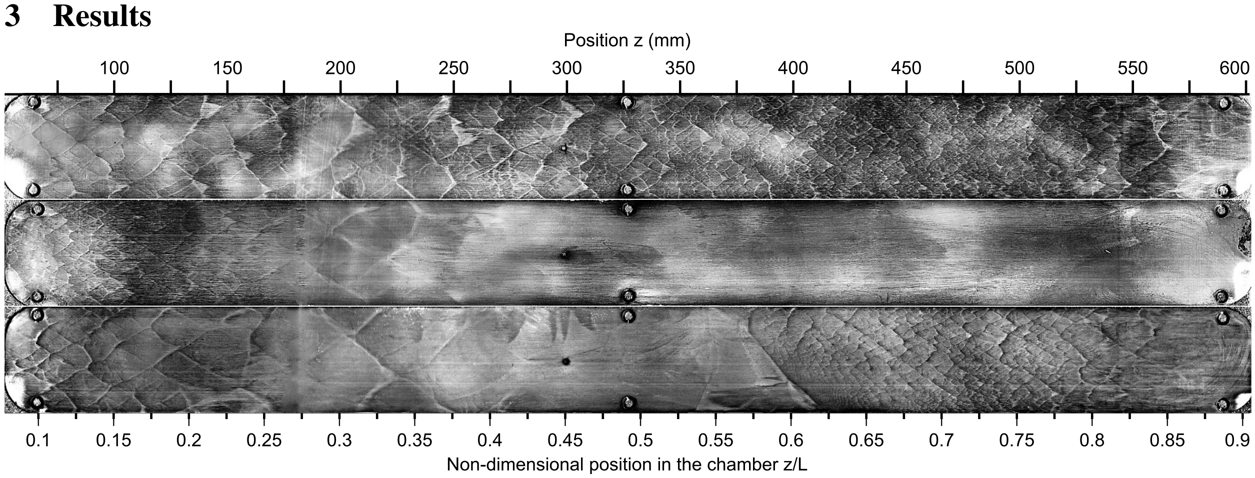

Figure 2: Sooted plate recordings of the transmission dynamics. Top: supercritical. Center: subcritical. Bottom: critical.

Figure 2 shows the dynamics of the transmission of an initially multicellular CJ detonation recorded on sooted plates for the three distributions in Figure 1 (right). These dynamics are:

1. the supercritical transmission (Fig. 2, top): the detonation continuously propagates as a multicellular CJ wave of which the mean cell width continuously adjusts to the local composition. This dynamics is obtained with the Supercritical-Gradient distribution (Fig. 1, curve 1) for which the reactivity sink is small.
2. the subcritical transmission (Fig. 2, center): the detonation suddenly fails (shock-flame decoupling) and does not re-initiate. This dynamics is obtained with the Subcritical-Gradient distribution (Fig. 1, curve 2) for which the reactivity sink is deep.
3. the critical transmission (Fig. 2, bottom): the detonation fails and re-initiates by means of a transverse detonation wave originating from the chamber walls. This dynamics is obtained with the Critical-Gradient distribution (Fig. 1, curve 3) for which the reactivity sink is intermediate between the last two ones.

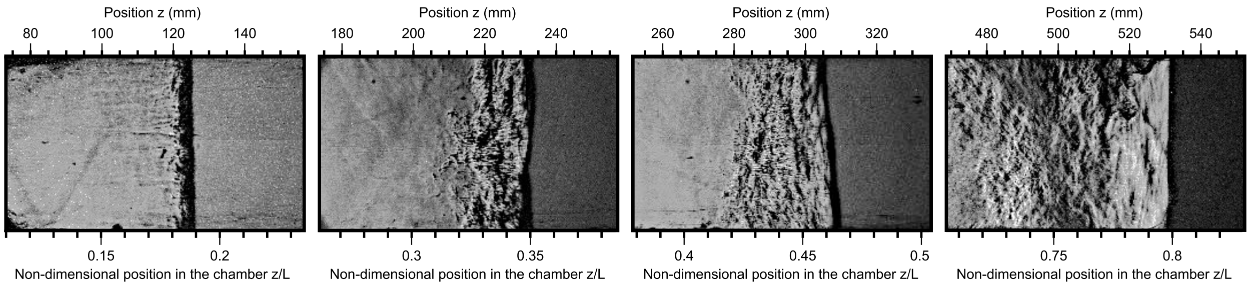

Figure 3: Subcritical transmission: Schlieren images of the detonation propagation and failure and of the combustion kernels generation.

Figure 3 shows four Schlieren frames of the subcritical transmission dynamics recorded in consecutive zones spanning the total length of the chamber ($L = 665$ mm). In the first frame, we observe a multicellular detonation front, characterized by a thin reaction layer with small cellular instabilities. In the second frame, we observe the shock-flame decoupling process, characterized by an increasingly large reaction layer and by the rapid damping of the cellular front structure. In the third frame, we observe the decoupled propagation, characterized by a large reaction layer that is separated from the shock by a non-reactive, shocked, layer of finite-thickness. In the fourth frame, after the local composition has returned reactive enough, we observe the formation of new combustion kernels. On Schlieren visualizations, this formation is identified by very dark spots characteristic of the very strong gradients associated with thin flame layers, as observed here in the vicinity of the top wall.

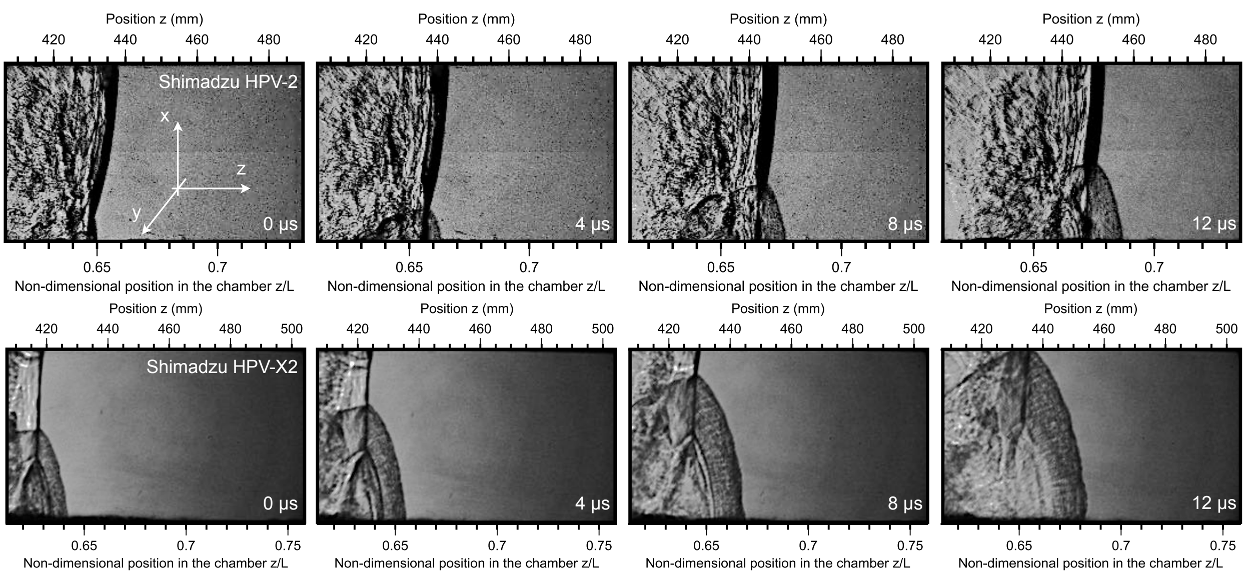

Figure 4: Critical transmission: Schlieren images of the detonation re-initiation process after failure.

Figure 4 shows two sequences (top and bottom rows) of four Schlieren frames of the detonation re-initiation process for the case of the critical transmission. These sequences were obtained in two experiments with different recording specifications (cf. Sect. 2). From the phenomenological viewpoint, the bottom sequence can be seen as the time continuation of the top one. As observed in Figure 2, bottom, the detonation re-initiates from the corner line of two orthogonal walls, in the form of a radially-diverging wave, with a very large number of transverse waves, that rapidly supersedes the decoupled shock and eventually reforms a quasi-planar multicellular detonation wave.

4 Discussion and conclusion

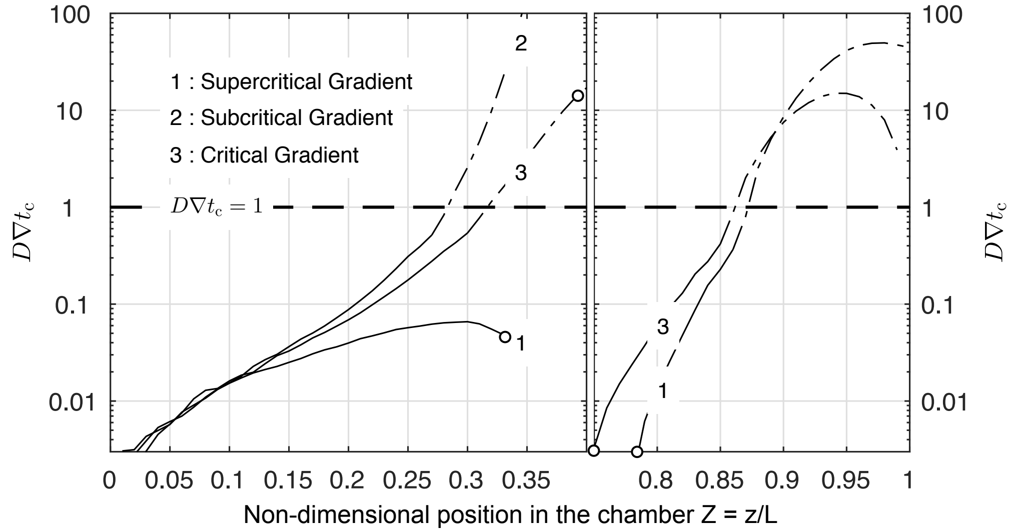

Figure 5: Variations of the criterion number $D\nabla t_c$ for shock-flame decoupling as function of the non-dimensional position z/L in domains of decreasing reactivity for the three considered gradients.

Gradient	Supercritical	Subcritical	Critical
Criterion: $D\nabla t_c > 1$	$Z \gtrsim 0.87$	$Z \gtrsim 0.29$	$Z \gtrsim 0.31$ and $Z \gtrsim 0.87$
Experiments: cells vanishing	$Z \approx 0.85$	$0.25 \lesssim Z \lesssim 0.3$	$0.3 \lesssim Z \lesssim 0.4$ and $0.8 \lesssim Z \lesssim 0.85$

Table 1: Comparisons of the positions where the shock-flame decoupling criterion (Fig. 5) is met to the positions where the cellular structure vanishes according to the experiments (Fig. 2).

Figure 5 shows the variation of the shock-flame decoupling criterion number $D\nabla t_c$ [11,12] along the chamber in the two domains of decreasing reactivity, i.e., for ER values ϕ such that $(1-\phi)\,\nabla\phi/\phi < 0$. The ZND characteristic time t_c was calculated by means of 1D planar steady ZND calculations with the San Diego chemical kinetics mechanism [17]. Table 1 compares the positions where the criterion $D\nabla t_c > 1$ is met (Fig. 5) to those where failure is experimentally observed (Fig. 2). The criterion is thus found to well predicts detonation failure and can therefore be considered as a reliable tool to assess the predictive capacity of numerical simulations to reproduce the dynamics of detonation in non-uniform compositions [12,13].

A failed detonation could re-initiate either as a deflagration (Fig. 3) or as a detonation (Fig. 4), depending essentially on the strength of the Mach reflections of residual transverse waves at the walls and on the capacity of the local mixture to accept the detonation regime. This detonation re-initiation could explain the transition to counter-rotating modes observed in RDEs [2,5] since, upon re-initiation, an explosive radial wave is generated and propagates in the two opposite directions of the propagation, i.e., the analog to the azimuthal direction of the RDE's annular chamber. Another way to stabilize the detonation regime in RDE chambers would be to force shock amplification along the detonation chamber by means of shock-focusing elements, e.g., obstacles positioned along the walls.

Acknowledgement

This work was funded by SAFRAN Aircraft Engines grant no. 920 653185 and the Association Nationale de la Recherche et de la Technologie (ANRT) grant no. CIFRE N°2013/1017. The authors are grateful to the CAPA research program on Alternative Combustion Mode for Air-breathing Propulsion supported by SAFRAN, MBDA Missiles systems and the Agence Nationale de la Recherche (ANR). We thank the Shimadzu company for letting us use their new camera model.

References

[1] Kasahara J., Frolov SM (2015). Present Status of Pulse and Rotating Detonation Engine Research. In 25th ICDERS, Leeds, UK.

[2] Rankin BA, Fotia ML, Naples AG, Stevens C, Hoke JL, Kaemming TA, Theuerkauf SW, Schauer FR (2017). Overview of Performance, Application, and Analysis of Rotating Detonation Engine Technologies. J. Prop. Power 33. 131–143.

[3] Brophy CM, Hanson RK (2006). Fuel distribution effects on Pulse Detonation Engine operation and performance. J. Prop. Power. 22(6). 1155–1161.

[4] Rankin BA, Fugger CA, Richardson DR, Cho KY, Hoke JL, Caswell AW, Gord JR, Schauer FR (2016). Evaluation of mixing processes in a non-premixed Rotating Detonation Engine using acetone PLIF imaging. AIAA SciTech. 1198.

[5] Burr J, Yu KH (2016). Detonation Reignition within a Rotating Detonation Engine. AIAA SciTech. 1202.

[6] Cocks PAT, Holley AT, Rankin BA (2016). High Fidelity Simulations of a Non-Premixed Rotating Detonation Engine. AIAA SciTech. 0125.

[7] Fujii J, Kumazawa Y, Matsuo A, Nakagami S, Matsuoka K, Kasahara J (2017). Numerical investigation on detonation velocity in rotating detonation engine chamber. Proc. Combust. Inst. 36(2). 2665–2672.

[8] Gaillard T (2017). Étude numérique du fonctionnement d'un moteur à détonation rotative. PhD thesis, Université Paris-Saclay.

[9] Boeck LR, Berger FM, Hasslberger J, Sattelmayer T (2016). Detonation propagation in hydrogen-air mixtures with transverse concentration gradients. Shock Waves 26. 181–192.

[10] Kuznetsov MS, Alekseev VI, Dorofeev SB, Matsukov ID, Boccio JL (1998). Detonation propagation, decay, and reinitiation in nonuniform gaseous mixtures. Proc. Combust. Inst. 27(2). 2241–2247.

[11] Boulal S, Vidal P, Zitoun R (2016). Experimental investigation of detonation quenching in non-uniform compositions. Combust. Flame 172. 222–233.

[12] Boulal S (2017). Comportements dynamiques de la détonation dans des compositions gazeuses non-uniformes. PhD thesis, École Nationale Supérieure de Mécanique et d'Aérotechnique.

[13] Matsumoto T, Boulal S, Matsuo A, Vidal P, Zitoun R (2017). Numerical investigation of detonation failure in non-uniform compositions and comparison to experiments. In 26th ICDERS, Boston, MA, USA.

[14] Mitrofanov VV, Soloukhin RI (1964). On the multifront detonation wave diffraction. Dokl. Akad. Nauk SSSR 159(5). 1003–1006.

[15] Bhattacharjee RR, Lau-Chapdelaine SSM, Maines G, Maley L, Radulescu MI (2013). Detonation re-initiation mechanism following the Mach reflection of a quenched detonation. Proc. Combust. Inst. 34(2). 1893–1901.

[16] Bach GG, Knystautas R, Lee JHS (1969). Direct initiation of spherical detonations in gaseous explosives. 12th Symp. (Int.) Combust. 853–864.

[17] Williams FA, Cattolica RJ, Seshadri K (2016). The San Diego Mechanism.